Muography of the Active Sakurajima Volcano: Recent Results and Future Perspectives of Hazard Assessment

László Oláh,[1,2] Hiroyuki K. M. Tanaka,[1,2] Takao Ohminato,[2] Gábor Nyitrai,[1,3] Gergő Hamar,[1,3] and Dezső Varga[1,3]

[1]*International Virtual Muography Institute (Global)*

[2]*Earthquake Research Institute, The University of Tokyo, Tokyo 113-0032, Japan*

[3]*Wigner Research Centre for Physics, Eötvös Loránd Research Network, Budapest 1121, Hungary*

Corresponding author: László Oláh
Email: olah.laszlo@wigner.hu

Abstract

Sakurajima volcano is one of the world's most active volcanoes with over 3,000 of explosive eruptions during the last five years. A muography observatory is under construction in international collaboration since 2017 at a distance of approx. 2,800 m in south-west direction from the active craters. Currently, the Sakurajima Muography Observatory is operating with 11 Multi-Wire-Proportional-Chamber-based Muography Observation Systems that are covering a sensitive surface area of 8.25 square meters. This work is focusing on the volcanological implications of muographic monitoring of Sakurajima: (i) tephra deposition, and erosion of the surface region exist due to heavy rains and post-eruptive lahars; (ii) magmatic plug formation was observed beneath the active craters after the deactivation of Showa crater in 2018 and after a dormant period of Central craters in 2020; (iii) machine-learning-based processing of daily muographic images achieved a fair area under the receiver operating characteristic curve score of 0.76.

Keywords: muography, volcano monitoring, tracking detector, machine learning, convolutional neural network
DOI: 10.31526/JAIS.2022.285

1. INTRODUCTION

Volcanic hazards globally endanger the landscapes, economies, and societies (approx. 10% of Earth's population). Most volcanic hazards (e.g., volcanic bombs, pyroclastic flows, tephra fall, etc.) are induced by the eruptions. However, some hazards, such as landslides or lahars (mud or debrish flows), can occur during the dormant periods. Various remote monitoring techniques are utilized for real-time observation of volcanic edifices. A nonexhaustive list of monitoring techniques from land to the atmosphere is provided as follows. (i) Video recording can measure the speed and direction of exploded ash (e.g., see [1]); (ii) synthetic aperture radars measure the deformation, either sinking or rising, of the crater floor (e.g., see [2, 3]); (iii) seismic techniques are used to reconstruct Earth's vibration even a few minutes prior to eruptions (e.g., see [4]); (iv) gas emission monitoring is applied to quantify the emission rates of volcanic gases (e.g., see [5]). The gaining of the amount of data and the possibility for real-time measurements encourage the application of machine learning techniques for either characterization or forecasting of volcanic phenomena.

Muography is a novel imaging technique that can measure mass density changes related to volcanic processes by means of the measurement of cosmic-ray muons penetrated through the volcanic edifice, e.g., see [6]. Since the 2010s, volcano observatories are under development in Americas [7, 8], Asia [9, 10, 11, 12, 13, 14, 15, 16], and Europe [17, 18, 19, 20, 21, 22]. In this work, we review the recent observations of the Multi-wire-proportional-chamber-based Muography Observation System (MMOS) [11, 23, 24] of Sakurajima Muography Observatory (SMO).

2. SAKURAJIMA MUOGRAPHY OBSERVATORY

The Sakurajima is an active stratovolcano located on the "Ring of fire" within the Aira caldera in Kagoshima Bay, Kyushu, Japan. The latest Plinian eruption occurred in 1914 and the next one is expected in the first half of the 21st century [25]. Two craters of the southern peak (the so-called Central craters and Showa crater) erupted consecutively in recent years. There are a few hundreds of (explosive) short-term eruptions per year. Short-term eruptions eject aerosols and gas with a bulk volume of below 10,000,000 m^3 to a height from 1,000 to 5,000 meters above the crater rims, throwing fragments of volcanic plug and lava bombs usually within approx. 3,000 m radius. Protection of tourists motivates the forecasting of short-term eruptions of the Sakurajima volcano.

Figure 1 shows the structure and data flow diagram of the MMOS. The MMOS is a modular instrument that is currently operating with eleven tracking systems in the SMO. Each tracking system is assembled from at least seven MWPCs. The size of MWPCs is 120 cm $\times$ 80 cm in six MMOSs and 80 cm $\times$ 80 cm in five MMOSs. Each detector provides two-dimensional positional information. The detector segmentation of 12 mm and the tracking system length of 200 cm allow an angular resolution of approx.

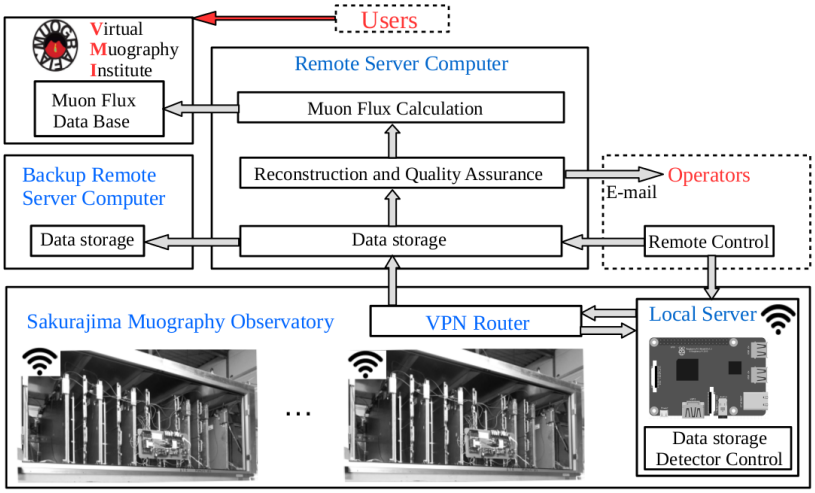

FIGURE 1: The schematic diagram of the MMOS.

3 mrad. The MMOS can spatially resolve the crater region with a resolution of below 10 meters from a distance of approx. 2,800 m. Five 2-cm-thick lead plates are installed between the detectors for background suppression. Currently, all the tracking systems are installed at the same location and oriented to 30.25° from North and 0° from horizon (Figure 2(A)). The data acquisition is controlled by microcomputers for each MMOS module. The modules communicate with a local server microcomputer that collects the data from all modules. These data are transferred to a remote server where automated track reconstruction and data quality assurance are performed based on a combinatorial algorithm [11]. The track count maps (muograms) are produced after the track selection, which is based on the goodness of track fits. The muograms are transferred to a database of the International Virtual Muography Institute [26]. An example of the measured flux map produced by off-line analysis is shown in Figure 2(B). An extensive description of the construction of MWPC-based tracking systems and the readout system are described in another article of this issue by Varga et al. [27].

3. OVERVIEW OF RECENT RESULTS

3.1. Muography of Hydrogeomorphic Changes on the Volcanic Edifice

Lahars are fast-moving gravity-driven flows of a mixture of volcanic rocks and water which occurred during either eruptions or dormant periods. Wind- and water-driven erosion processes can destabilize and mobilize the tephra deposition before they become fully incorporated into the soil. The generation and dynamics of lahars are controlled by the (i) local topography, (ii) volcanic activity, (iii) amount and composition of tephra, and (iv) intensity and duration of rainfall. Muography has the potential to measure the amount (mass and thickness) of tephra deposition [14, 15] and topographical changes that control the onset of post-eruptive lahars [15].

Muon flux was monitored through the Central Craters (CC), Showa and Arimura Basin (SAB), Arimura Middle Reaches (AMR), and two reference regions (RR1 and RR2). These regions are shown in Figure 2(B). The fluxes were averaged in each angular region for time intervals of 4 days, and the averaged fluxes were smoothed by applying a moving average calculated from the previous ten consecutive time intervals, i.e., over a period of 40 days. After September 2019, the relative averaged fluxes (measured relatively the flux of the first time sequence, F0) decreased through the volcano regions from 10 to 40% (Figure 3) [15].

The mass was derived with the procedure detailed in [15]. Figure 4 shows the variations of total mass relative to M0 with 1σ errors (green bands), the daily number of lahars (orange impulses), the daily total precipitation (blue impulses), and hourly maximum precipitation (red impulses), as well as the daily frequency of eruptions that occurred from the Central Crater vents (yellow impulses) [15]. There was a change of volcanic ejecta mass that was measured to approx. 0.25 Mt between April and September 2019 and approx. 2 Mt from September 2019 to July 2020 by the Japan Meteorological Agency. The total mass (volcanic edifice and tephra) was measured to M0 $= (7.54 \pm 0.05)$ Mt for the 1st time-interval. Mass deposit showed significantly decreasing trends through various periods, e.g., from November 2019 to January 2020, during March 2020 and October 2020. The interpretation of the observation is the following:

(i) The volcanic sediments were transported from the selected peak regions to downstream regions of the volcano by the onset of rain-triggered lahar events (Figure 4(A)).

(ii) The onsets of lahars were triggered by the heavy rainfalls with hourly maximum precipitation of above 10 mm per hour instead of the total daily precipitation (Figure 4(B)).

(iii) Further mass decreases were observed without the occurrence of lahar events, e.g., after mid-September 2020. This observation suggests the water-driven erosion of the peak region of Sakurajima volcano.

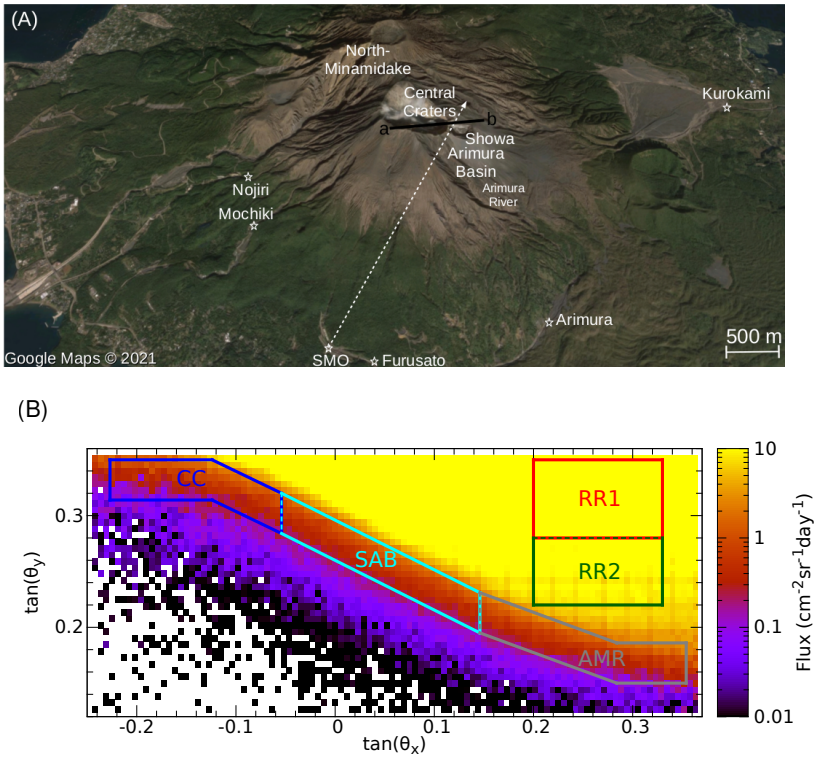

FIGURE 2: The measurement arrangement. (A) The map of the measurement site with the location and orientation (dashed white line) of MMOS (source: Google Maps). (B) An example of the measured flux by the MMOS [15].

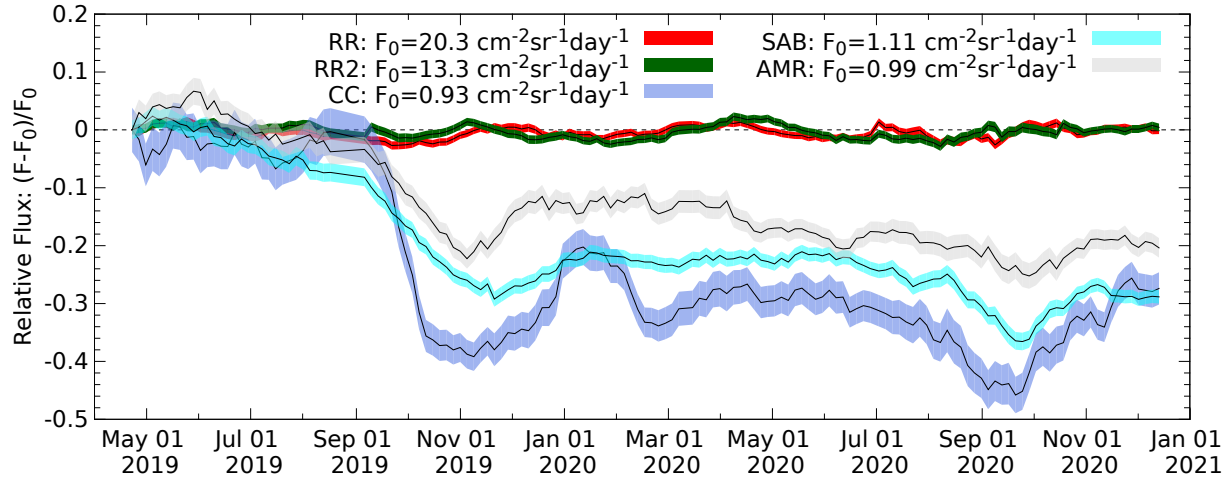

FIGURE 3: The relative flux variations are shown as a function of time for the two Reference Regions (red and dark-green bands), Central Craters (blue band), Showa Crater and Arimura Basin (cyan band), and Arimura Middle Reaches (gray band), respectively [15]. The variations of averaged muon fluxes (F) were measured relatively to the fluxes measured for the 1st period (F0).

(iv) The mass deposition rate did not correlate with the eruption frequency and the amount of ejected materials per eruption is larger when the interval between the eruptions is longer (Figure 4(C)). These are consistent with the observations of an earlier measurement campaign [28].

Our observations demonstrate that muography can measure the hydrogeomorphic changes that occurred due to erosion processes at a shorter duration. Muographic monitoring can improve the modeling of erosion of volcanic edifices and assessment of hazard levels.

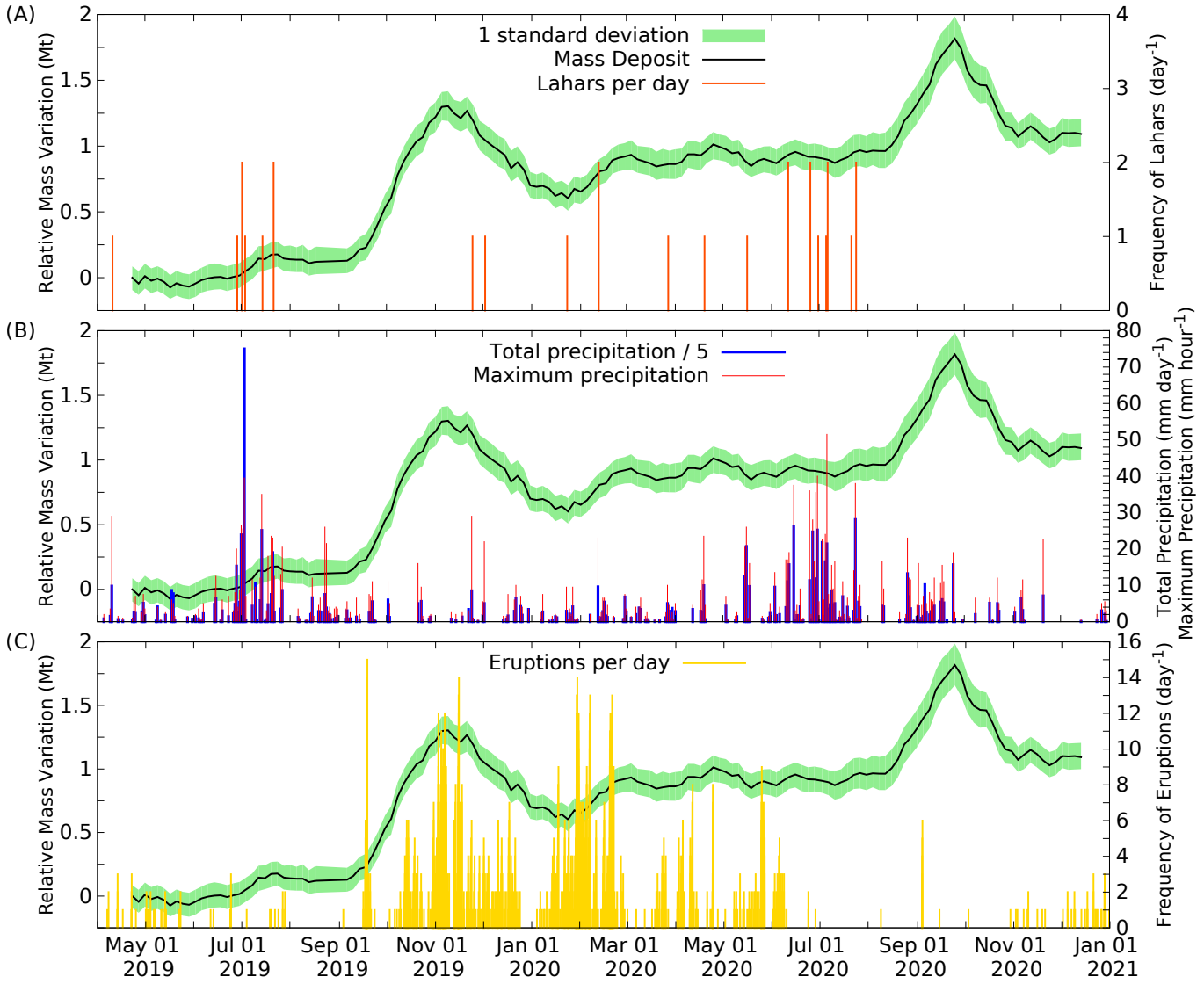

FIGURE 4: The relative mass variations (green error bands) are shown as a function of time and compared to the variations of the daily number of lahar events (orange impulses in panel A), total daily precipitation (blue impulses in panel B), maximum hourly precipitation (red impulses in panel B), and the daily number of eruptions (yellow impulses in panel C) [15]. The variations of averaged masses (M) were measured relatively to the masses measured for the 1st period (M-M0).

3.2. Muography of the Intrusion of Magmatic Materials beneath the Active Craters

Muographic imaging allows observing various volcanic phenomena in association with the subsurface movements of magmatic materials [9]: the shape of the magma bodies either intruded or deposited, empty pathways, degassing processes, and ascent and descent of magma.

During the measurement period from January 2017 to June 2018, we observed the formation of a magmatic plug underneath the deactivated Showa crater with three MMOS modules [12]. The eruptive activity of the Central craters has also decreased significantly after February 2020: 310 explosions occurred on 182 days from September 2019 to March 2020 and 69 explosions occurred on 291 days from March 2020 to December 2020. A similar analysis was performed for investigating the overlying phenomena. Figure 5 shows the corresponding density images for the crater region as a function of horizontal and vertical track slopes with a bin size of 0.23 mrad by 23 mrad [29]. The solid black line shows a cross-section of the crater region along the a-b line of Figure 2(A). We have investigated the density variations underneath the Central crater with the currently obtained data and found that there was a significant density reduction right beneath the crater floor. If we define the density derived for the period before the eruptions was deactivated to be ρ_1 and that after the eruption were deactivated to be ρ_2, $(\rho_2 - \rho_1)/\Delta\rho_{1,\mathrm{lower}}$ ranged from 1.45 to 1.84 in bins within the region surrounded by blue dashed lines in Figure 5. As a result, the average density was reduced from 1.68 g/cm^3 to 1.37 g/cm^3 in this region. This picture is consistent with our previous model constructed for the Sakurajima eruption mechanism [29]: a volcanic plug is formed and continued to evolve during the active eruption period, but once it is deactivated, the volcanic

plug is no longer formed or evolved. The corresponding mass change is approximated to 7.5 Mt. The observation suggests that magma intrusion temporarily plugged the Central craters. Besides muographic observation, the presence of magmatic materials was also suggested by the incandescence of the crater that was observed at night during the dormant periods of the volcano [30].

Based on the muographic observations of the active craters of the Sakurajima volcano, the existence of a low-density, debris-filled volume is assumed under the two craters. This volume acts as a magma reservoir with a lateral extension of approx. 300 m at depth of 100–200 m. Liquid magma fills the intergrain spaces in this volume a few tens of minutes before the onset of the eruption. After the eruption, the liquid magma is drained back into the conduit. Thereafter, the solidification of this volume creates a magmatic plug under the crater. The deactivation of the Showa crater and the latest dormant periods of Central craters were due to the decrease in the permeability of the magma reservoir.

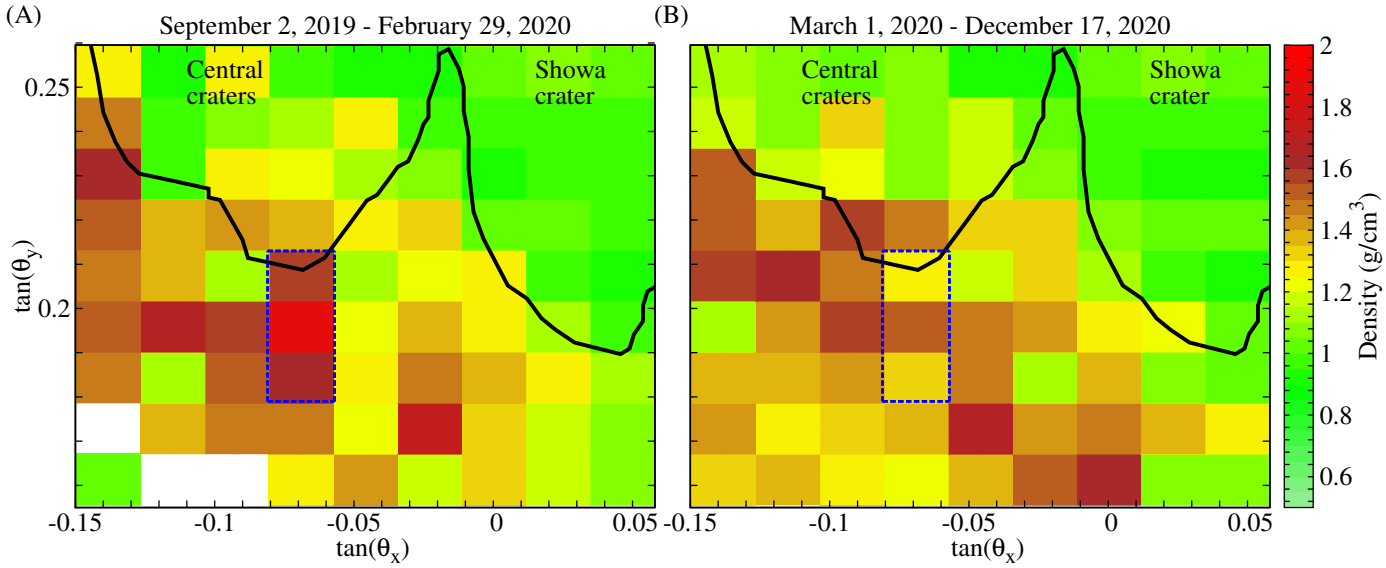

FIGURE 5: The densities measured through the craters are shown for the period before (A) and during (B) the dormant periods of the Sakurajima volcano. The white-shaded regions have no density values due to the lack of muon counts during the data collection period. The solid black line shows the cross-section along the a-b line of Figure 2(A). The blue dashed lines highlight the angular regions with a significant density increase [29].

3.3. Volcano Eruption Forecasting with Muography

Machine learning [34] of time series data collected by a volcano monitoring technique can be utilized for classifying volcanic events and forecasting short-term volcanic eruptions, e.g., see [31, 32]. We applied the concept of Nomura et al. [13] and developed our methods for forecasting the eruptions of the Central craters of Sakurajima volcano with muographic images captured by the MMOS [33]. Figure 6 shows the schematic drawing of the concept using a convolutional neural network (CNN) model. For this study, the flux of penetrating particles was calculated for 24-hour time periods. The daily muograms were determined with an angular bin size of 23 mrad that could resolve the volcanic edifice with a spatial resolution of 60 m. The CNN was applied for processing the subimages extracted from three regions, the active Central craters, the dormant Showa crater, and the surface region [33], for a period from October 2018 to June 2020. Furthermore, an eruption label was determined for each daily muogram: "1" if at least one eruption occurred, else "0".

The data set was divided into three parts for training, validating, and testing the CNN model. Adams' methods was applied for hyperparameter tunning of the CNN model [35]. The Receiver Operating Characteristic (ROC) analysis was applied for evaluating the performance of the model. Figure 7 shows the ROC curves for the Central craters (red line), a crater (green line), and surface region (blue line). The cutoff points of the ROC curves were chosen with the Youden's index [36]. The sensitivity (true positive rate) is determined by the ratio of the number of forecasted eruptions to the total number of eruptions. The specificity (1-false positive rate) is corresponding to the rate of fake forecasts. As was expected, the active Central craters had a higher Area Under the ROC Curve (AUC) than the dormant Showa crater and the surface region. Despite the application of an upgraded muography observation system with enlarged (from 5 m^2 to 8.25 m^2) sensitive surface area and higher angular resolution (from 33 mrad to

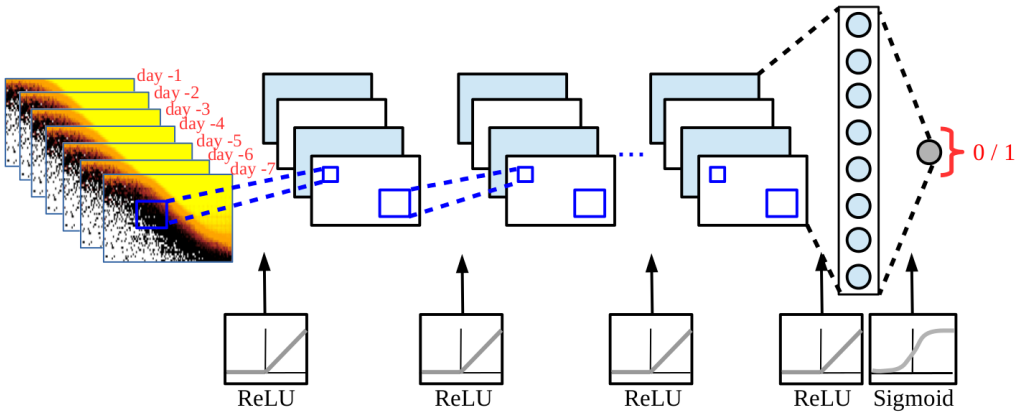

FIGURE 6: The schematic drawing of a convolutional neural network-based model applied for eruption forecasting [33]. Seven consecutive daily muographic images were processed with CNN using Rectified Linear Unit (ReLU) activation functions. A fixed filter size of 3×3 was used in this analysis. The output of CNN was processed with a fully connected neural network with a Sigmoid activation function and the output neuron provided 2-bit information for the occurrence of the eruption on the 8th day.

23 mrad), the ROC AUC was not drastically improved, specifically 0.76 by our study and 0.72 by Nomura et al., due to the following reasons:

(i) Fewer eruptions occurred in the Central craters (832) than in Showa (1432) that resulted in a smaller amount of training data,

(ii) Smaller amount of mass was transported underneath the Central craters than in Showa that resulted in smaller variations in muographic images,

(iii) The geometrical difference between the two craters is also assumed to be an influencing factor.

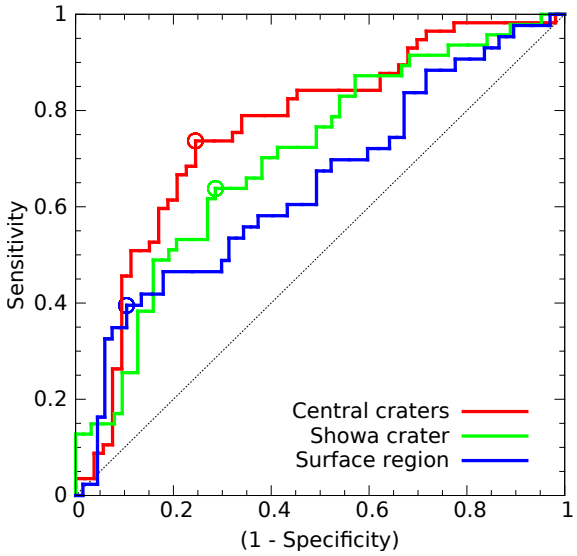

FIGURE 7: The ROC curve of convolutional neural network model for volcano eruption prediction [33].

The application of more sophisticated approaches, e.g., Recurrent Neural Network with Long-Short-Term Memory [37], is expected to improve the current forecasting performances.

4. SUMMARY AND FUTURE PERSPECTIVES

We demonstrated the applicability of the MMOS of SMO for observation of hydrogeomorphic changes, and subsurface movements of magmatic materials. Our muographic image processing methods achieved a fair ROC AUC score of 0.76 for eruption prediction. The upgrade of MMOS is a prerequisite to improve time resolution and spatial resolution of muographic imaging. For improvement

of the forecasting of short-term eruptions, the combination of muographic data with the data of conventional volcano monitoring techniques is planned.

CONFLICTS OF INTEREST

The authors declare that there are no conflicts of interest regarding the publication of this paper.

ACKNOWLEDGMENTS

This work is supported by the Joint Usage Research Project (JURP) of the University of Tokyo, Earthquake Research Institute (ERI) under project ID 2020-H-05, the "INTENSE" H2020 MSCA RISE project under Grant Agreement No. 822185, the Hungarian NKFIH research grants under ID OTKA-FK-135349 and TKP2021-NKTA-10, Wigner Research Centre for Physics of the Eötvös Loránd Research Network, and the Ministry of Education, Culture, Sports, Science and Technology, Japan (MEXT) Integrated Program for the Next Generation Volcano Research. The technical support provided by the members of the REGARD group is gratefully acknowledged.

References

[1] A. J. C. Witsil and J. B. Johnson, Volcano video data characterized and classified using computer vision and machine learning algorithms. Geoscience Frontiers **11**, 1789–1803, *https://doi.org/10.1016/j.gsf.2020.01.016* (2020).
[2] Y. Aoki et al., L-band Synthetic Aperture Radar: Current and future applications to Earth sciences. Earth, Planets and Space **73**, 56, *https://doi.org/10.1186/s40623-021-01363-x* (2021).
[3] N. Anantrasirichai et al., Application of Machine Learning to Classification of Volcanic Deformation in Routinely Generated InSAR Data. Journal of Geophysical Research: Solid Earth **123**, 6592–6606, *https://doi.org/10.1029/2018JB015911* (2018).
[4] R. Ortiz et al., Volcanic and volcano-tectonic activity forecasting: a review on seismic approaches. Annals of Geophysics **62**, VO06, *https://doi.org/10.4401/ag-7655* (2019).
[5] R. Kazahaya et al., Pre-eruptive inflation caused by gas accumulation: insight from detailed gas flux variation at Sakurajima volcano, Japan. Geophys. Res. Lett. 43, 11219–11225. *https://doi.org/10.1002/2016gl070727* (2016).
[6] L. Oláh, H. K. M. Tanaka, and D. Varga, Muography: Exploring Earth's Subsurface with Elementary Particles, Geophysical Monograph **270**, ISBN 9781119723028, American Geophysical Union, John Wiley & Sons, Inc. (2022).
[7] A. Vesga-Ramírez et al., Muon tomography sites for Colombian volcanoes. Annals of Geophysics **63**, 6, VO661.*https://doi.org/10.4401/ag-8353* (2020).
[8] J. Peña-Rodríguez et al. Design and construction of MuTe: A hybrid Muon Telescope to study Colombian volcanoes. JINST **15**, P09006 *https://doi.org/10.1088/1748-0221/15/09/P09006* (2020).
[9] H. K. M. Tanaka, Japanese volcanoes visualized with muography. Philosophical Transactions of the Royal Society A **377** 20180142 *https://doi.org/10.1098/rsta.2018.0142* (2019).
[10] R. Nishiyama et al., 3D density modeling with gravity and muon-radiographic observations in Showa-Shinzan lava dome, Usu, Japan. Pure and Applied Geophysics **174**, 1061–1070 *https://doi.org/10.1007/s00024-016-1430-9* (2017).
[11] L. Oláh, H. K. M. Tanaka, T. Ohminato, and D. Varga, High-definition and low-noise muography of the Sakurajima volcano with gaseous tracking detectors. Scientific Reports **8(3207)**, *https://doi.org/10.1038/s41598-018-21423-9* (2018).
[12] L. Oláh et al., Plug Formation Imaged Beneath the Active Craters of Sakurajima Volcano With Muography. Geophysical Research Letters **46** 10417–10424 *https://doi.org/10.1029/2019GL084784* (2019).
[13] Y. Nomura et al., Pilot study of eruption forecasting with muography using convolutional neural network. Scientific Reports **10** 5272 *https://doi.org/10.1038/s41598-020-62342-y* (2020).
[14] H. K. M. Tanaka, Development of the muographic tephra deposit monitoring system. Scientific Reports **10(14820),** *https://doi.org/10.1038/s41598-020-71902-1* (2020).
[15] L. Oláh, H. K. M. Tanaka, and G. Hamar, Muographic monitoring of hydrogeomorphic changes induced by post-eruptive lahars and erosion of Sakurajima volcano. Sci Rep **11** 17729 *https://doi.org/10.1038/s41598-021-96947-8* (2021).
[16] S. Miyamoto et al., A muographic study of a scoria cone from 11 directions using nuclear emulsion cloud chambers.Geosci. Instrum. Method. Data Syst. Discuss., preprint, *https://doi.org/10.5194/gi-2021-35* (2021).
[17] J. Marteau et al., DIAPHANE: Muon tomography applied to volcanoes, civil engineering, archaelogy. JINST **12**, C02008, *https://doi.org/10.1088/1748-0221/12/02/C02008* (2017).
[18] V. Tioukov et al., First muography of Stromboli volcano. Scientific Reports **9**, 6695, *https://doi.org/10.1038/s41598-019-43131-8* (2019).
[19] D. Lo Presti, Muographic monitoring of the volcano-tectonic monitoring evolution of Mount Etna. Scientific Reports **10**, 11351. *https://doi.org/10.1038/s41598-020-68435-y* (2020).
[20] A. Barnoud et al., Robust Bayesian joint inversion of gravimetric and muographic data for the density imaging of the Puy de Dôme Volcano (France). Frontiers in Earth Science **8**, 575842, *https://doi.org/10.3389/feart.2020.575842* (2021).
[21] G. Macedonio et al., Muography of the volcanic structure of the summit of Vesuvius. In: L. Oláh, H. K. M. Tanaka, & D. Varga (Eds.), Muography: Exploring Earth's Subsurface with Elementary Particles, Geophysical Monograph Series **270** 123–136 *https://doi.org/10.1002/9781119722748.ch09* (2022).
[22] C. D. Athanassas, Muography for geological hazard assessment in the South Aegean active volcanic arc (SAAVA). Mediterranean Geoscience Reviews, *https://doi.org/10.1007/s42990-020-00020-x* (2020).
[23] D. Varga et al., High efficiency gaseous tracking detector for cosmic muon radiography. Advances in High Energy Physics **2016** 1962317 *https://doi.org/10.1155/2016/1962317* (2016).
[24] D. Varga et al., Detector developments for high performance muography applications. Nuclear Instruments and Methods in Physics Research Section A **958**, 162236. *https://doi.org/10.1016/j.nima.2019.05.077* (2020).

[25] J. Hickey et al., Thermomechanical controls on magma supply and volcanic deformation: application to Aira caldera, Japan. Scientific Reports **6**, 32691, *https://doi.org/10.1038/srep32691* (2016).
[26] Muogram viewer of International Virtual Muography Institute, Retrieved from https://mmos.muographers.org/ (Last view on 17/01/2022).
[27] D. Varga et al., Construction and readout systems for gaseous muography detectors, Journal of Advanced Instrumentation in Science 2022 No. 1. (2022).
[28] T. Kusagaya, Reduction of background noise in muographic images for detecting magma dynamics in an active volcano. Phd Thesis, The University of Tokyo *https://doi.org/10.15083/00077464* (2017).
[29] L. Oláh and H. K. M. Tanaka, Muography of Magma Intrusion Beneath the Active Craters of Sakurajima Volcano, Japan. In: L. Oláh, H. K. M. Tanaka, & D. Varga (Eds.), Muography: Exploring Earth's Subsurface with Elementary Particles, Geophysical Monograph Series **270** 109–122 *https://doi.org/10.1002/9781119722748.ch08* (2022).
[30] A. E. Crafford and E. Venzke, Report on Aira (Japan). Bulletin of the Global Volcanism Network **45**, 7, *https://doi.org/10.5479/si.GVP.BGVN202007-282080* (2020).
[31] M. E. Gaddes, A. Hooper, and M. Bagnardi, Using Machine Learning to Automatically Detect Volcanic Unrest in a Time Series of Interferograms. Journal of Geophysical Research: Solid Earth **124**, 12304–12322, *https://doi.org/10.1029/2019JB017519* (2019).
[32] M. G. Whitehead and M. S. Bebbington, Method selection in short-term eruption forecasting. Journal of Volcanology and Geothermal Research **419**, 107386 *https://doi.org/10.1016/j.jvolgeores.2021.107386* (2021).
[33] L. Oláh and H. K. M. Tanaka, Machine Learning with Muographic Images as Input: An Application to Volcano Eruption Forecasting. In: L. Oláh, H. K. M. Tanaka, & D. Varga (Eds.), Muography: Exploring Earth's Subsurface with Elementary Particles, Geophysical Monograph Series **270** 43–54 *https://doi.org/10.1002/9781119722748.ch04* (2022).
[34] A. Géron, Hands-on Machine Learning with Scikit-Learn, Keras & TensorFlow, ISBN 9781492032649, O'Reilly Media (2019).
[35] D. P. Kingma and L. J. Ba, Adam: A Method for Stochastic Optimization. International Conference on Learning Representations, *https://arxiv.org/abs/1412.6980v5* (2015).
[36] W. J. Youden, Index for rating diagnostic tests. Cancer **3**, 3235, *https://doi.org/10.1002/1097-0142* (1950).
[37] S. Hochreiter and J. Schmidhuber, Long short-term memory. Neural Computation **9**, 1735-1780, *https://doi.org/10.1162/neco.1997.9.8.1735* (1997).